JOURNAL OF MOLECULAR SPECTROSCOPY **130**, 33–45 (1988)

High-Resolution Laser Spectroscopy of Strontium Monomethoxide, $SrOCH_3$

L. C. O'BRIEN, C. R. BRAZIER, AND P. F. BERNATH[1]

Department of Chemistry, University of Arizona, Tucson, Arizona 85721

The rotational analysis of the 0–0 band of the $\tilde{A}^2E_{3/2}$–$\tilde{X}^2A_1$ transition of the $SrOCH_3$ free radical has been carried out by laser excitation spectroscopy. The $SrOCH_3$ molecule was found to have C_{3v} symmetry with a Sr–O bondlength of 2.12 Å. There was no evidence of a Jahn–Teller effect in the $\tilde{A}^2E$ state. This work is the first high-resolution analysis of a metal alkoxide molecule.

INTRODUCTION

We have recently observed the gas-phase low-resolution (1 cm^{-1}) spectra of many new alkaline earth metal containing free radicals (*1–7*), including $SrOCH_3$. These molecules are made by the reaction of alkaline earth atoms (Ca, Sr, or Ba) with alcohols (*1, 2*), carboxylic acids (*1*), isocyanic acid (*3*), cyclopentadiene (*4*), metal alkyls (*5*), amines (*6*), and acetylene (*7*). The free radical product molecule contains one alkaline earth metal atom and one ligand group.

Low-resolution spectra of alkaline earth monomethoxides were first reported by Wormsbecher and Suenram (*8*). In these experiments $SrOCH_3$ was produced by the gas-phase reaction of strontium atoms with methyl nitrite, CH_3ONO. A vibrational analysis of the $\tilde{A}^2E$–$\tilde{X}^2A_1$ and $\tilde{B}^2A_1$–$\tilde{X}^2A_1$ transitions was reported.

There are several recent high-resolution analyses of SrOH (*9, 10*) as well as other alkaline earth monohydroxides, MgOH (*11*), CaOH (*12–14*), and BaOH (*15*). We report here the first high-resolution analysis of a metal monomethoxide. The 0–0 band of the $\tilde{A}^2E$–$\tilde{X}^2A_1$ transition of $SrOCH_3$ was recorded by laser excitation spectroscopy with narrowband fluorescence detection. A high-resolution analysis is in progress for similar molecules such as $SrNH_2$, SrN_3, SrNCO, CaC_2H, $CaCH_3$, and SrSH by Bernath and co-workers.

There has been some theoretical interest in ^2E electronic states due to the possibility of Jahn–Teller interactions (*16–20*). There are only two molecules for which a ^2E electronic state has previously been studied at high resolution: CH_3O (*21–24*) and FSO_3 (*25*). The methoxy radical work is relevant to this study in terms of both the analysis of a ^2E state and the structural information, which can be transferred to $SrOCH_3$.

The Sr–O–C bond angle in $SrOCH_3$, like the Sr–O–H bond angle, is found to be 180°, and thus $SrOCH_3$ is a prolate symmetric top of C_{3v} symmetry. The $\tilde{A}^2E$ state

[1] Alfred P. Sloan Fellow.

0022-2852/88 $3.00

has a large spin–orbit splitting similar to the value of 263 cm^{-1} for the corresponding $\tilde{A}^2\Pi$ state of SrOH. The off-axis hydrogens in $SrOCH_3$ do not perturb the spin–orbit coupling in the $\tilde{A}^2E$ state. The $\tilde{A}^2E$ state exhibits a strong first-order Coriolis interaction between the orbital angular momentum and the rotational angular momentum. There is no experimental evidence of a Jahn–Teller distortion of $SrOCH_3$ in the $\tilde{A}^2E$ state.

METHOD

The production of $SrOCH_3$ in a Broida oven (*26*) has been described previously (*2*). Briefly, Sr metal was vaporized from a resistively heated alumina crucible and entrained in a flow of Ar carrier gas (~1 Torr). Methanol is an easier oxidant to use than the methyl nitrite used by Wormsbecher and Suenram (*8*). However, the methyl nitrite–strontium reaction produces more strontium monomethoxide than the methanol–strontium reaction since it is more exothermic. When excited strontium atoms ($^3P_1$ Sr) are used for the reaction with methanol, a large amount of $SrOCH_3$ is produced, sufficient for the present study.

Two dye laser systems were used. The 5-W all lines output of a Coherent Innova 90-4 argon ion laser was used to pump a broadband (~1 cm^{-1}) Coherent 599-01 dye laser operated from 6600 to 7000 Å with DCM dye. Either the 4880 or the 5145 Å output of a Coherent Innova 20 argon ion laser was used to pump a single mode (~1 MHz) Coherent 699-29 computer-controlled ring dye laser operated near 6760 and 6890 Å with DCM dye and LD 688 dye, respectively. The two output beams from the dye lasers were spatially overlapped and focused into the Broida oven. The output from one of the dye lasers was always tuned to the $^3P_1$–$^1S_0$ Sr atomic line at 6892 Å. The $SrOCH_3$ laser-induced fluorescence signal was increased by 3 orders of magnitude when excited $^3P_1$ Sr was used as a reactant. The other dye laser was used to probe for the reaction product, $SrOCH_3$.

For preliminary survey work, the low-resolution laser excitation spectrum was recorded by tuning the ring dye laser to the Sr atomic line and scanning the broadband laser (1 cm^{-1}) while detecting the laser-induced fluorescence through a red-pass filter (Schott RG 780).

Low-resolution resolved fluorescence spectra were recorded by tuning one laser to the Sr atomic line and the other laser to the $SrOCH_3$ transition. The emission was focused onto the slits of a 0.64-m monochromator and detected with a cooled photomultiplier tube (RCA C31034) using photon counting electronics.

High-resolution laser excitation spectra with narrow band-pass detection were recorded to observe the rotational structure (for example, (*27*)). For all high-resolution spectra the broadband laser was tuned to the Sr atomic transition.

The P_{21} and Q_2 bandheads (the splitting of the two heads is too small to be resolved) of the $^2E_{3/2}$–$^2A_1$ spin component were recorded by setting the monochromator (0.8 cm^{-1} resolution) in the P_2 branch and scanning the ring laser through the connecting P_{21} and Q_2 branches. The notation for a $^2\Pi$–$^2\Sigma$ transition, as described by Herzberg (*28*), will be used for this Hund's case (a) ^2E–$^2A_1$ transition. The monochromator acts as a narrowband-pass filter to select the rotational levels connected to the P_{21} and Q_2 bandheads. Since the different K subbands have nearly the same origin (similar to a parallel transition), the P_2 rotational lines of different K subbands are badly overlapped.

This proved useful in recording the P_{21} and Q_2 bandheads. When the monochromator was set in the P_2 branch, P_{21} and Q_2 bandheads of 10 to 20 K subbands were recorded in a single scan (Fig. 1).

Individual rotational lines of the $^2E_{3/2}$–$^2A_1$ component were recorded by setting the monochromator on the P_{21} and Q_2 bandheads of a single subband (0.3 cm^{-1} resolution). In these experiments the monochromator acts as a narrowband-pass filter to select rotational levels belonging to a single subband.

An iodine cell was used to calibrate the wavemeter of the computer-controlled dye laser. The absolute accuracy of our line positions is approximately ± 0.005 cm^{-1}.

RESULTS AND DISCUSSION

A. Electronic Structure

Low-resolution laser excitation scans were recorded for $SrOCH_3$ in the region 6000–8200 Å. These spectra show vibronic structure belonging to two electronic transitions, $\tilde{B}^2A_1$–$\tilde{X}^2A_1$ and $\tilde{A}^2E$–$\tilde{X}^2A_1$. Figure 2 is a low-resolution laser excitation spectrum of the $\tilde{A}^2E$–$\tilde{X}^2A_1$ transition. The $\tilde{A}^2E$–$\tilde{X}^2A_1$ transition is analogous to the $\tilde{A}^2\Pi$–$\tilde{X}^2\Sigma^+$ transition of the linear SrOH, which is in turn analogous to the $A^2\Pi$–$X^2\Sigma^+$ transition of the strontium monohalides. The bonding in $SrOCH_3$, like SrOH and SrX, is very ionic, Sr^+–$^-OCH_3$, and there is one nonbonding valence electron. For the ground electronic state this electron is in the metal-centered $5s(a_1)$ orbital, and the electronic transition involves the promotion of this valence electron to the $4d$-$5p(e)$ metal-centered hybrid orbitals.

The $\tilde{A}^2E$ state has a spin–orbit splitting of 267.5 cm^{-1}, thus the $^2E_{1/2}$ and $^2E_{3/2}$ components are well separated and the $\tilde{A}^2E$ state exhibits Hund's case (a) coupling. Hund's case (a) coupling for a ^2E state has been described in detail by Brown (*18*). $\hat{\mathbf{L}}$, $\hat{\mathbf{S}}$, $\hat{\mathbf{R}}$, and $\hat{\mathbf{J}}$ are the orbital angular momentum, spin angular momentum, rotational angular momentum, and the total angular momentum (exclusive of nuclear spin), respectively. The ^2E state is strongly Hund's case (a), and the projections of $\hat{\mathbf{N}}$, $\hat{\mathbf{S}}$, and $\hat{\mathbf{J}}$ are quantized along the prolate top axis as K, Σ, and P, respectively, with $P = K + \Sigma$. The projection of $\hat{\mathbf{L}}$ on the top is $\zeta_e d$. For a ^2E–$^2A_1$ transition the selection rules are $\Delta K = \pm 1$, $\Delta J = 0, \pm 1$.

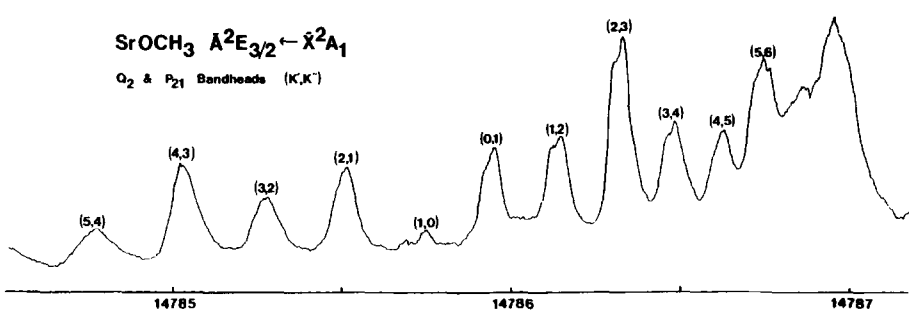

FIG. 1. Laser excitation spectrum of the strontium monomethoxide O_0^0 $\tilde{A}^2E_{3/2}$–$\tilde{X}^2A_1$ transition. The blue degraded Q_2 and P_{21} bandheads form a "head of heads" near 14 787 cm^{-1}.

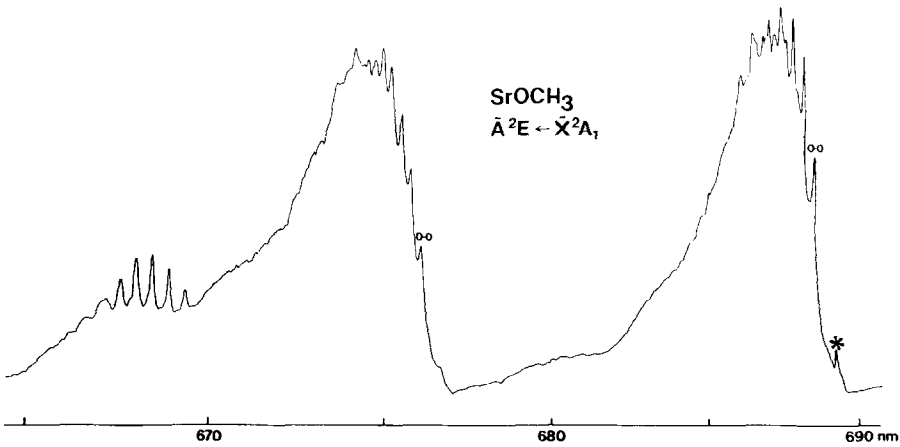

FIG. 2. Low-resolution laser excitation spectrum of the $\tilde{A}^2E$–$\tilde{X}^2A_1$ transition in strontium monomethoxide. The broad feature to the blue is the $\tilde{A}^2E_{3/2}$–$\tilde{X}^2A_1$ transition while the $\tilde{A}^2E_{1/2}$–$\tilde{X}^2A_1$ feature lies between 680 and 690 nm. The sharp feature marked 0–0 is the Q_2 and P_{21} bandheads of the O_0^0 $\tilde{A}^2E$–$\tilde{X}^2A_1$ electronic transition.

$\zeta_e d$ corresponds to Λ in the linear SrOH case with $\Lambda = \pm 1$ for the corresponding $\tilde{A}^2\Pi$ electronic state. The presence of the off-axis hydrogens can quench the projection of the orbital angular momentum, so usually $\zeta_e(SrOCH_3) < \Lambda(SrOH)$. However, the hydrogens are far from the unpaired electron, which is located on the strontium atom, and very little quenching was expected. The Jahn–Teller effect also quenches the orbital angular momentum through the d portion of the $\zeta_e d$ parameter. The small difference in the spin–orbit splitting in SrOH and $SrOCH_3$ is consistent with $\zeta_e \sim 1$. For linear SrOH,

$$E_{SO} = A\Lambda\Sigma, \qquad \text{where} \qquad A = 263.5\ \text{cm}^{-1},$$

while for the symmetric top $SrOCH_3$, only the product $a\zeta_e d$ can be determined,

$$E_{SO} = a\zeta_e d\Sigma, \qquad \text{where} \qquad a\zeta_e d = 267.5\ \text{cm}^{-1}.$$

B. Vibrational Structure

Since the electronic transitions involve nonbonding orbitals, there is little change in the geometry in the different electronic states of $SrOCH_3$. As a result, the sequence structure is very compact and the Franck–Condon factors are quite diagonal. The bands involving the Sr–O stretch have the largest Franck–Condon factors because this mode is associated with the metal atom.

$SrOCH_3$ has 12 normal modes, 4 of a_1 symmetry and 4 degenerate pairs of e symmetry, for a total of 8 vibrations. These vibrations have the following approximate description: ν_1 (a_1 symmetry) is the CH_3 symmetric stretch; ν_2 (a_1) is the CH_3 symmetric bend; ν_3 (a_1) is the C–O stretch; ν_4 (a_1) is the Sr–O stretch; ν_5 (e) is the CH_3 asymmetric stretch; ν_6 (e) is the CH_3 asymmetric bend; ν_7 (e) is the O–CH_3 wag; and ν_8 (e) is the Sr–O–C bend.

The observed vibrational frequencies are listed in Table I with estimated experimental uncertainties of ± 5 cm^{-1}. Several weak ground state vibrational frequencies were detected by exciting the ^2E–$^2A_1$ 0–0 transition and resolving the fluorescence with a monochromator. The two modes which appear most strongly, ν_4 and ν_3, have been assigned and reported previously (*2, 7*). The weak feature corresponding to a vibration of 1450 cm^{-1} is assigned to ν_2, the CH_3 symmetric bend of a_1 symmetry. There is one alternative assignment to this feature, that of the ν_6 CH_3 asymmetric bend of e symmetry. This latter assignment was considered because the two modes in CH_3OH which correspond to ν_6 occur at 1475 and 1455 cm^{-1}. We prefer the ν_2 assignment because of symmetry considerations. Within the Born–Oppenheimer approximation for an electric dipole allowed electronic transition, $\Delta v = 1$ for vibrations of a_1 symmetry are allowed while $\Delta v = 1$ for an e mode is forbidden (*29*). The vibronic feature corresponding to a 271 cm^{-1} vibration was assigned to $2\nu_8$, the Sr–O–C bend. Although ν_8 is of e symmetry, transitions involving two quanta in this vibration are allowed (*29*).

C. *Rotational Structure*

$SrOCH_3$ is a prolate symmetric top and we use the $\hat{\mathbf{N}}^2$ form of the rotational Hamiltonian developed by Brown (*18*), extended by Hougen (*19*), and as explicitly described by Endo *et al.* (*23*);

$$\hat{\mathbf{H}}_{\mathrm{ROT}} = (A - B)\hat{\mathbf{N}}_z^2 + B\hat{\mathbf{N}}^2,$$

where $\hat{\mathbf{N}} = \hat{\mathbf{J}} - \hat{\mathbf{S}}$. Centrifugal distortion constants were needed,

$$\hat{\mathbf{H}}_{\mathrm{CD}} = -D_N\hat{\mathbf{N}}^4 - D_{NK}\hat{\mathbf{N}}^2\hat{\mathbf{N}}_z^2 - D_K\hat{\mathbf{N}}_z^4.$$

The first-order electronic Coriolis interaction was also included for the ^2E state

$$\hat{\mathbf{H}}_{\mathrm{COR}} = -2A\hat{\mathbf{N}}_z\hat{\mathbf{L}}_z + \eta_e\hat{\mathbf{N}}^2\hat{\mathbf{N}}_z\hat{\mathbf{L}}_z + \eta_K\hat{\mathbf{N}}_z^3\hat{\mathbf{L}}_z.$$

TABLE I

Vibrational Frequencies of $SrOCH_3$

State	mode	frequency (cm^{-1})
$\tilde{X}^2A_1$	ν_2 (CH_3 sym. bend, a_1)	1450
	ν_3 (C-O stretch, a_1)	1138
	ν_4 (Sr-O stretch, a_1)	405
	$2\nu_4$	809
	$\nu_3 + \nu_4$	1545
	$2\nu_8$ (Sr-O-C bend)	271
$\tilde{A}^2E$	ν_3 (C-O stretch, a_1)	1140, 1150[a]
	ν_4 (Sr-O stretch, a_1)	418, 415[a]

[a] Reference 8.

The energy levels in the E state are split into $(+l)$ and $(-l)$ stacks by this coupling as explained by Herzberg (*29*). The leading Coriolis term in the Hamiltonian provides a diagonal matrix element of $-2A\zeta_l K$. The effect of this interaction changes the origin of the different K subbands, and when $\zeta_l = 1$ all subbands have nearly the same origin. Although the ^2E–$^2A_1$ transition is formally a perpendicular transition ($\Delta K = \pm 1$), it has the appearance of a parallel transition and thus is very compact (*29*).

The spin–rotation interaction was included in the ground state Hamiltonian:

$$\hat{\mathbf{H}}_{SR} = \epsilon_{aa}\hat{\mathbf{N}}_z\hat{\mathbf{S}}_z + 1/4(\epsilon_{bb} + \epsilon_{cc})(\hat{\mathbf{N}}_+\hat{\mathbf{S}}_- + \hat{\mathbf{N}}_-\hat{\mathbf{S}}_+).$$

ϵ_{aa} was not well determined since this term is significant only for low J lines which could not be detected.

For the excited state, the spin–orbit interaction was included with the term

$$\hat{\mathbf{H}}_{SO} = a\hat{\mathbf{L}}_z\hat{\mathbf{S}}_z,$$

which produces a diagonal matrix element $a\zeta_e d\Sigma$. All of the matrix elements of the various terms in the Hamiltonian are explicitly listed by Endo *et al.* (*23*). For the $^2A_1$ state, the matrix elements for $\hat{\mathbf{H}}_{COR}$ and $\hat{\mathbf{H}}_{SO}$ are set to zero.

The 0–0 band of the $\tilde{A}^2E_{3/2}$–$\tilde{X}^2A_1$ transition was recorded at high resolution and analyzed. The $\tilde{A}^2E_{1/2}$–$\tilde{X}^2A_1$ spin component was too compact and the individual rotational lines were unassignable. All the transitions were measured using the monochromator as a narrowband filter to simplify the spectra.

The $\tilde{A}^2E_{3/2}$–$\tilde{X}^2A_1$ transition has six branches per K subband. These are spaced by approximately "$-3B$" (P_2), "$-B$" (P_{21} and Q_2), "$+B$" (Q_{21} and R_2), and "$+3B$" (R_{21}) at low J, and the $-B$ and $+B$ branches are doubled due to the spin–rotation interaction in the ground state. Spin–rotation doubling was resolved in the $+B$ branch. No sign of j-type doubling was observed (analogous to Λ-type doubling in a Π state) because no transitions connecting to $K' = 1$ in the $^2E_{1/2}$ component were recorded. Individual rotational lines were recorded in all of the branches except for the $-B$ branch.

Figure 1 is a high-resolution laser excitation spectrum of the 0_0^0 $-B$ bandheads recorded through the monochromator. This is a high-resolution scan of the peak marked 0–0 in the low-resolution $^2E_{3/2}$–$^2A_1$ spectrum in Fig. 2. K' and K'' are given above each bandhead. The $-3B$ and $-B$ branches form blue degraded bandheads. The $-B$ bandheads of different K subbands are very close together due to the first-order Coriolis interaction and actually form a red degraded "head of heads" as shown. The bandhead intensities are not reliable so the ($K' = 2$, $K'' = 3$) $-B$ bandhead appears to be the most intense because of the placement of the monochromator filter.

The effect of nuclear spin statistics of the three equivalent hydrogens are clearly shown (Fig. 1) by the 2:1:1:2 intensity alternation of different K subbands. The intensity of a subband is doubled for $K'' = 0, 3, 6, \ldots$. The ground state K'' assignment was straightforward. The $-1B$ bandheads were recorded by detecting fluorescence in the $-3B$ branches (Fig. 1). The $K' = 1 - K'' = 0$ subbandhead appears weak (Fig. 2) because for this subband there is no connection between the $-3B$ and $-B$ branches (like a $^2\Pi$–$^2\Sigma^+$ transition). The $-3B$ and $-B$ branches terminate on rotational states of different symmetry (parity) in the excited state, separated by j doubling (like Λ doubling). For all other subbands, both these symmetry components (A_1 and A_2, or E) are equally populated by the laser because for $K'' \neq 0$ the ground state rotational

levels are degenerate (A_1 and A_2 or E, see Ref. (*29*, p. 91)). Thus, the $-3B$ and $-B$ branches appear in the excitation spectrum. This assignment was also consistent with the nuclear spin statistics for the other K subbands.

There remain two possible assignments for the remaining bands, either p or r type in K. The data were fit using both possible excited state K' assignments. One choice was eliminated because the ground state K-stack origins determined from the fit were physically unreasonable.

The observed $SrOCH_3$ transition wavenumbers which were used in the fit are listed in Table II. A sample spectrum of individual P-branch lines is shown in Fig. 3. Lines from six different subbands were recorded [$(K', K'') = (10, 9), (7, 6), (4, 3), (0, 1), (1, 0), (2, 3)$]. Low J lines could not be observed due to the badly overlapped subbands. Six hundred and twenty lines were fit with 14 parameters with a standard deviation of 0.003 cm^{-1}, close to the estimated measurement error. The molecular constants determined are given in Table III.

The values of the parameters a (spin–orbit), ζ_e ($\langle \Lambda | L_z | \Lambda \rangle$), and d (Jahn–Teller quenching) are completely correlated so the product $\zeta_e d$ was set to the value of 1 in the fit. Since the $^2E_{1/2}$ spin component was not rotationally analyzed, the value of the spin–orbit constant, a, was adjusted to reproduce the location of the 0–0 $^2E_{1/2}$–$^2A_1$ subbandheads observed at high resolution. The values of ζ_e and d are expected to be less than or equal to 1 so the value of the spin–orbit constant in $SrOCH_3$ (267.53 cm^{-1}) is slightly larger than the corresponding SrOH value of 263.52 cm^{-1}.

The constants A', a, and ζ_l are also correlated and cannot be simultaneously determined. For the final fit A'' was set to 5.1851 cm^{-1}, the value Endo *et al.* (*23*) observed for CH_3O. The parameter ζ_l was badly correlated with other parameters so it was fixed to the value of 1.

There is no experimental evidence for a Jahn–Teller effect in the $\tilde{A}^2E$ state of $SrOCH_3$. The vibrational structure for the Jahn–Teller active mode ν_8, the Sr–O–C bend, displayed the selection rule $\Delta v_8 = \pm 2$ not $\Delta v_8 = \pm 1$. The molecular parameters derived from the rotational structure have reasonable values consistent with the assumptions $\zeta_e d$ and $\zeta_l = 1$.

The $\tilde{A}^2E$ state in $SrOCH_3$ is quite different from the $\tilde{X}^2E$ state of OCH_3. The electronic structure of the $\tilde{A}^2E$ state of $SrOCH_3$ can be viewed as a nonbonding, unpaired electron in a $p\pi$-$d\pi$ orbital polarized away from a Sr^{2+} core. The large Sr^{2+} core separates the closed-shell $^-OCH_3$ ligand from the unpaired electron. The three off-axis hydrogens are thus far away from the unpaired electron. The unpaired electron sees a locally linear environment resulting in a spin–orbit coupling constant similar to SrOH and an unobservably small Jahn–Teller effect. The unpaired electron does not communicate with the three hydrogen atoms.

The rotational structure of $SrOCH_3$ is consistent with a C_{3v} geometry for both $\tilde{A}^2E$ and $\tilde{X}^2A_1$ electronic states. The covalent CH_3OH molecule has C_s symmetry, but if the H atom bonding to the oxygen is replaced by a more electronegative atom such as Li or Na, ab initio calculations predict a C_{3v} structure (*30, 31*).

The electronic charge distribution is M^+–$^-OCH_3$ with some delocalization of the negative charge over the CH_3 group. Calculations on CH_3O^- predict (*32*) that the O^- donates electrons into an unoccupied π^* orbital on the carbon atom. This interaction shortens the O–C bond, lengthens the C–H bonds, and decreases the H–C–H angle.

TABLE II

Observed Transitions in the $\tilde{A}^2E$–$\tilde{X}^2A_1$ Band of $SrOCH_3$ (cm^{-1})

a

K'= 0, K"= 1

J	$P_2(J)$		$Q_{21}(J)$		$R_2(J)$		$R_{21}(J)$	
23.5			14 790.173	-0.004	14 790.326	-0.008		
24.5			14 790.326	0.010	14 790.468	-0.006		
25.5			14 790.453	-0.001	14 790.609	-0.007		
26.5			14 790.594	-0.002	14 790.749	-0.012		
27.5	14 781.380	-0.002	14 790.743	0.002	14 790.905	-0.004		
28.5	14 781.190	-0.001	14 790.893	0.006	14 791.050	-0.008		
29.5	14 781.004	0.000	14 791.036	0.001	14 791.211	0.002		
30.5	14 780.821	0.004	14 791.184	-0.001	14 791.365	0.002		
31.5	14 780.635	0.002	14 791.338	0.000	14 791.523	0.005	14 796.867	0.000
32.5	14 780.449	-0.000	14 791.495	0.002	14 791.682	0.005	14 797.189	-0.002
33.5	14 780.269	-0.000	14 791.650	0.000	14 791.837	0.001	14 797.517	-0.000
34.5	14 780.094	0.002	14 791.817	0.007	14 792.000	0.002	14 797.847	0.000
35.5	14 779.916	-0.000	14 791.969	-0.001	14 792.168	0.005	14 798.177	-0.001
36.5	14 779.742	-0.001	14 792.139	0.005	14 792.336	0.006	14 798.513	0.001
37.5	14 779.575	0.002	14 792.306	0.005	14 792.501	0.003	14 798.844	-0.002
38.5	14 779.403	0.000	14 792.471	0.003	14 792.667	-0.001	14 799.182	-0.003
39.5	14 779.236	-0.000	14 792.636	-0.002	14 792.841	-0.000	14 799.526	0.000
40.5	14 779.071	-0.001	14 792.811	0.000	14 793.011	-0.005	14 799.863	-0.004
41.5	14 778.905	-0.004	14 792.991	0.006	14 793.191	-0.003	14 800.208	-0.003
42.5	14 778.747	-0.003	14 793.164	0.003	14 793.370	-0.004	14 800.558	-0.000
43.5	14 778.592	-0.000	14 793.343	0.002	14 793.558	0.002	14 800.907	-0.000
44.5	14 778.436	0.000	14 793.523	0.002	14 793.740	-0.000	14 801.255	-0.003
45.5	14 778.285	0.001	14 793.711	0.006	14 793.925	-0.001	14 801.608	-0.003
46.5	14 778.136	0.004	14 793.892	0.001	14 794.123	0.008	14 801.962	-0.004
47.5	14 777.983	0.000	14 794.073	-0.004	14 794.304	-0.001	14 802.321	-0.002
48.5	14 777.834	-0.001	14 794.264	-0.003	14 794.509	0.010	14 802.679	-0.004
49.5	14 777.689	-0.002	14 794.455	-0.004	14 794.692	-0.000	14 803.045	-0.000
50.5	14 777.549	0.000	14 794.655	0.001			14 803.408	-0.000
51.5	14 777.406	-0.003	14 803.772	-0.003				
52.5			14 804.140	-0.004				

b

K'= 2, K"= 3

J	$P_2(J)$		$Q_{21}(J)$		$R_2(J)$		$R_{21}(J)$	
21.5					14 790.433	0.001		
22.5			14 790.418	0.004	14 790.570	0.002		
23.5			14 790.552	0.002	14 790.705	-0.000		
24.5			14 790.691	0.005	14 790.845	-0.000		
25.5			14 790.829	0.002	14 790.988	0.000		
26.5			14 790.970	0.002	14 791.133	0.000		
27.5	14 781.760	0.005	14 791.118	0.006	14 791.280	0.000		
28.5	14 781.567	0.003	14 791.262	0.004	14 791.429	-0.000		
29.5	14 781.378	0.002	14 791.409	0.002	14 791.579	-0.001		
30.5	14 781.190	0.000	14 791.560	0.004	14 791.735	0.001		
31.5	14 781.003	-0.001	14 791.710	0.001	14 791.887	-0.002		
32.5	14 780.821	-0.001	14 791.867	0.003	14 792.046	-0.001		
33.5	14 780.641	-0.001	14 792.024	0.003	14 792.206	-0.001		
34.5	14 780.461	-0.003	14 792.182	0.002	14 792.366	-0.003		
35.5	14 780.287	-0.002	14 792.336	-0.005	14 792.531	-0.002		
36.5	14 780.114	-0.002	14 792.505	-0.000	14 792.696	-0.004		
37.5	14 779.944	-0.001	14 792.669	-0.001	14 792.866	-0.002		
38.5	14 779.773	-0.002	14 792.840	0.000	14 793.036	-0.004		
39.5	14 779.607	-0.002	14 793.005	-0.004	14 793.213	-0.000		
40.5	14 779.443	-0.001	14 793.179	-0.002	14 793.389	-0.000	14 800.238	-0.000
41.5	14 779.280	-0.003	14 793.353	-0.003	14 793.562	-0.004	14 800.578	-0.005
42.5	14 779.121	-0.001	14 793.531	-0.002	14 793.746	0.000	14 800.928	-0.001
43.5	14 778.967	0.001	14 793.713	0.001	14 793.932	0.004	14 801.277	-0.001
44.5	14 778.810	0.000	14 793.895	0.002	14 794.114	0.001	14 801.628	-0.000
45.5	14 778.658	0.001	14 794.078	0.001	14 794.305	0.007	14 801.985	0.002
46.5	14 778.508	0.002	14 794.264	0.001	14 794.494	0.006	14 802.336	-0.001
47.5	14 778.359	0.002	14 794.452	0.002	14 794.681	0.003	14 802.691	-0.004
48.5	14 778.210	0.000	14 794.647	0.007	14 794.872	0.001	14 803.052	-0.003
49.5	14 778.065	-0.000	14 794.839	0.007	14 795.062	-0.003	14 803.414	-0.002
50.5	14 777.923	-0.000	14 795.027	0.001			14 803.775	0.005
51.5	14 777.782	-0.000					14 804.142	-0.004
52.5							14 804.513	-0.001
53.5							14 804.884	-0.001
54.5							14 805.257	-0.000
55.5							14 805.632	-0.000
56.5							14 806.013	0.002
57.5							14 806.393	0.004
58.5							14 806.774	0.004
59.5							14 807.162	0.008

TABLE II—*Continued*

c

K'= 4, K"= 3

J	$P_2(J)$		$Q_{21}(J)$		$R_2(J)$		$R_{21}(J)$	
18.5	14 782.250	-0.002						
19.5	14 782.040	-0.001	14 788.831	-0.015				
20.5	14 781.833	-0.000	14 788.831	0.000	14 788.966	-0.011		
21.5	14 781.626	-0.000	14 788.966	0.004	14 789.100	-0.012		
22.5	14 781.425	0.001	14 789.100	0.005	14 789.238	-0.009		
23.5	14 781.221	0.000	14 789.238	0.008	14 789.375	-0.011		
24.5	14 781.018	-0.003	14 789.375	0.007	14 789.522	-0.004	14 793.706	0.001
25.5	14 780.824	0.000	14 789.518	0.011	14 789.663	-0.005	14 794.015	0.000
26.5	14 780.627	-0.001	14 789.653	0.004	14 789.815	0.001	14 794.325	-0.001
27.5	14 780.434	-0.001	14 789.798	0.005	14 789.960	-0.000	14 794.640	-0.000
28.5	14 780.246	0.000	14 789.945	0.006	14 790.112	0.001	14 794.957	0.000
29.5	14 780.057	0.000	14 790.092	0.004	14 790.265	0.003	14 795.277	0.002
30.5	14 779.870	0.000	14 790.240	0.002	14 790.421	0.005	14 795.594	-0.001
31.5	14 779.687	0.000	14 790.392	0.001	14 790.576	0.004	14 795.918	-0.000
32.5	14 779.502	-0.002	14 790.551	0.004	14 790.732	0.003	14 796.246	0.002
33.5	14 779.320	-0.004	14 790.702	-0.000	14 790.893	0.003	14 796.573	0.002
34.5	14 779.145	-0.002	14 790.863	0.000	14 791.051	-0.000	14 796.902	0.001
35.5	14 778.970	-0.001	14 791.026	0.001	14 791.219	0.003	14 797.232	0.000
36.5	14 778.798	-0.000	14 791.191	0.003	14 791.383	-0.000	14 797.566	0.000
37.5	14 778.628	0.000	14 791.351	-0.002	14 791.555	0.002	14 797.899	-0.002
38.5	14 778.459	0.000	14 791.521	-0.000	14 791.723	-0.000	14 798.234	-0.004
39.5	14 778.289	-0.003	14 791.691	-0.001	14 791.900	0.003	14 798.580	0.000
40.5	14 778.126	-0.002	14 791.867	0.001	14 792.070	-0.002	14 798.920	-0.002
41.5	14 777.966	-0.000	14 792.037	-0.003	14 792.250	0.000	14 799.267	0.000
42.5	14 777.807	0.000	14 792.212	-0.004	14 792.430	0.000	14 799.615	0.001
43.5	14 777.649	-0.000	14 792.392	-0.003	14 792.612	0.000	14 799.962	-0.000
44.5	14 777.495	0.001	14 792.574	-0.003	14 792.796	-0.000	14 800.312	-0.001
45.5	14 777.340	-0.000	14 792.759	-0.001	14 792.986	0.002	14 800.669	0.002
46.5	14 777.188	-0.001	14 792.946	-0.000			14 801.023	0.001
47.5	14 777.040	-0.001					14 801.379	-0.001
48.5	14 776.895	0.000					14 801.739	-0.001
49.5	14 776.751	0.001					14 802.104	0.002
50.5	14 776.610	0.001					14 802.464	-0.001
51.5	14 776.471	0.002					14 802.831	-0.001
52.5	14 776.331	0.000					14 803.200	-0.001
53.5	14 776.196	0.000					14 803.574	0.001
54.5	14 776.059	-0.003						
55.5	14 775.928	-0.004						
56.5	14 775.797	-0.005						

d

K'= 7, K"= 6

J	$P_2(J)$		$Q_{21}(J)$		$R_2(J)$		$R_{21}(J)$	
13.5	14 782.464	-0.006						
14.5	14 782.252	0.002						
15.5	14 782.044	0.013						
16.5	14 781.814	0.000						
17.5	14 781.592	-0.006						
18.5	14 781.384	-0.002			14 787.838	-0.010		
19.5	14 781.170	-0.005	14 787.838	0.004	14 787.970	-0.008	14 791.309	-0.010
20.5	14 780.965	-0.002	14 787.970	0.007	14 788.101	-0.008	14 791.620	0.002
21.5	14 780.760	-0.001	14 788.101	0.008	14 788.235	-0.009	14 791.909	-0.010
22.5	14 780.558	0.000	14 788.235	0.008	14 788.372	-0.008	14 792.221	-0.001
23.5	14 780.358	0.001	14 788.372	0.009	14 788.502	-0.017	14 792.524	-0.003
24.5	14 780.158	0.000	14 788.502	0.001	14 788.650	-0.009	14 792.841	0.005
25.5	14 779.961	0.000	14 788.650	0.010	14 788.797	-0.005	14 793.145	-0.001
26.5	14 779.766	0.000	14 788.797	0.014	14 788.940	-0.007	14 793.453	-0.004
27.5	14 779.572	-0.000	14 788.940	0.014	14 789.080	-0.014	14 793.767	-0.005
28.5	14 779.382	-0.000	14 789.080	0.007	14 789.236	-0.009	14 794.084	-0.005
29.5	14 779.190	-0.003	14 789.236	0.013	14 789.389	-0.007	14 794.407	-0.000
30.5	14 779.005	-0.003	14 789.389	0.016	14 789.542	-0.007	14 794.729	0.000
31.5	14 778.823	-0.001	14 789.542	0.016	14 789.704	-0.002	14 795.051	-0.000
32.5	14 778.645	0.001	14 789.686	0.004	14 789.864	-0.000	14 795.373	-0.003
33.5	14 778.467	0.002	14 789.838	-0.001	14 790.024	-0.001	14 795.703	-0.001
34.5	14 778.286	-0.000	14 790.003	0.004	14 790.188	-0.000	14 796.034	-0.000
35.5	14 778.113	0.000	14 790.164	0.003	14 790.353	-0.000	14 796.369	0.002
36.5	14 777.939	-0.000	14 790.328	0.003	14 790.521	0.000	14 796.702	0.002
37.5	14 777.769	0.000	14 790.496	0.005	14 790.692	0.001	14 797.038	0.001
38.5	14 777.601	-0.000	14 790.663	0.003	14 790.862	0.000	14 797.376	0.001
39.5	14 777.434	-0.001	14 790.828	-0.002	14 791.032	-0.003	14 797.715	-0.000
40.5	14 777.272	0.000	14 791.003	-0.000	14 791.214	0.002	14 798.053	-0.005
41.5	14 777.111	0.000	14 791.177	-0.002	14 791.390	0.000	14 798.400	-0.003
42.5	14 776.955	0.004	14 791.355	-0.001	14 791.574	0.003	14 798.749	-0.001
43.5	14 776.799	0.004	14 791.537	0.001	14 791.757	0.004	14 799.101	0.000
44.5	14 776.642	0.002	14 791.714	-0.004	14 791.937	-0.000	14 799.453	0.001
45.5	14 776.488	0.001	14 791.902	0.000	14 792.126	0.001	14 799.806	0.000
46.5	14 776.337	-0.000	14 792.086	-0.002	14 792.314	0.000	14 800.161	-0.000
47.5	14 776.188	-0.000	14 792.276	-0.000	14 792.504	-0.000	14 800.520	0.000
48.5	14 776.040	-0.003	14 792.466	-0.001	14 792.698	-0.000	14 800.879	-0.001

TABLE II—*Continued*

d

K'= 7, K"= 6

J	$P_2(J)$		$Q_{21}(J)$		$R_2(J)$		$R_{21}(J)$	
49.5	14 775.900	0.000	14 792.661	0.001	14 792.898	0.003	14 801.240	-0.002
50.5	14 775.758	-0.000	14 792.857	0.001	14 793.098	0.005	14 801.607	-0.000
51.5	14 775.620	0.000	14 793.050	-0.002	14 793.300	0.007	14 801.976	0.001
52.5	14 775.481	-0.001	14 793.254	0.001			14 802.341	-0.002
53.5	14 775.344	-0.003					14 802.711	-0.003
54.5	14 775.216	0.000					14 803.083	-0.004
55.5	14 775.084	-0.000						
56.5	14 774.961	0.003						

e

K'= 10, K"= 9

J	$P_2(J)$		$Q_{21}(J)$		$R_2(J)$		$R_{21}(J)$	
21.5	14 779.773	-0.001						
22.5	14 779.572	-0.000			14 787.382	-0.008		
23.5	14 779.372	0.001	14 787.378	0.006	14 787.530	0.000		
24.5	14 779.171	-0.001	14 787.517	0.006	14 787.665	-0.005		
25.5	14 778.975	-0.000	14 787.657	0.006	14 787.809	-0.005		
26.5	14 778.782	0.000	14 787.797	0.003	14 787.962	0.002		
27.5	14 778.588	-0.002	14 787.945	0.007	14 788.104	-0.003	14 792.784	0.002
28.5	14 778.404	0.003	14 788.092	0.007	14 788.254	-0.003	14 793.096	-0.003
29.5	14 778.215	0.001	14 788.239	0.004	14 788.402	-0.007	14 793.416	-0.00
30.5	14 778.030	0.002	14 788.387	0.001	14 788.564	0.000	14 793.743	0.003
31.5	14 777.845	-0.000	14 788.546	0.006	14 788.723	0.001	14 794.060	-0.003
32.5	14 777.664	-0.000	14 788.704	0.008	14 788.878	-0.002	14 794.389	0.000
33.5	14 777.487	0.001	14 788.856	0.002	14 789.046	0.005	14 794.716	-0.000
34.5	14 777.307	-0.002	14 789.024	0.010	14 789.208	0.003	14 795.050	0.003
35.5	14 777.134	-0.001	14 789.185	0.007	14 789.365	-0.005	14 795.376	-0.002
36.5	14 776.960	-0.003	14 789.345	0.003	14 789.536	-0.001	14 795.711	-0.002
37.5	14 776.794	0.000	14 789.516	0.007	14 789.710	0.002	14 796.050	-0.000
38.5	14 776.625	-0.002	14 789.678	0.000	14 789.883	0.003	14 796.390	0.000
39.5	14 776.461	-0.000	14 789.853	0.003			14 796.729	-0.001
40.5	14 776.298	-0.001	14 790.023	0.000	14 790.234	0.002	14 797.072	-0.002
41.5	14 776.137	-0.001	14 790.202	0.002	14 790.412	0.001	14 797.417	-0.003
42.5	14 775.980	-0.000	14 790.375	-0.002	14 790.592	0.000	14 797.762	-0.005
43.5	14 775.826	0.001	14 790.567	0.009	14 790.767	-0.007	14 798.112	-0.005
44.5	14 775.671	0.000			14 790.961	0.000	14 798.465	-0.005
45.5	14 775.519	-0.000	14 790.929	0.003	14 791.148	-0.001	14 798.821	-0.003
46.5	14 775.372	0.002	14 791.116	0.003	14 791.339	0.000	14 799.180	-0.001
47.5	14 775.220	-0.002	14 791.304	0.002	14 791.535	0.003	14 799.540	-0.000
48.5	14 775.079	0.000	14 791.489	-0.003	14 791.726	0.000	14 799.905	0.003
49.5	14 774.933	-0.002	14 791.685	-0.002	14 791.925	0.002	14 800.267	0.002
50.5	14 774.794	-0.001	14 791.881	-0.001	14 792.120	-0.001	14 800.633	0.002
51.5	14 774.657	-0.001	14 792.080	-0.001	14 792.323	0.000		
52.5	14 774.521	-0.000	14 792.270	-0.011	14 792.529	0.002		
53.5	14 774.391	0.002	14 792.472	-0.012				
54.5	14 774.255	-0.001						
55.5	14 774.129	0.000						
56.5	14 774.001	-0.000						
57.5	14 773.874	-0.003						

f

K'= 1, K"= 0

J	$R_{21}(J)$	
31.5	14796.660	0.007
32.5	14796.980	0.001
33.5	14797.312	0.007
34.5	14797.641	0.007
35.5	14797.969	0.003
36.5	14798.303	0.004
37.5	14798.638	0.003
38.5	14798.969	-0.004
39.5	14799.311	-0.003
40.5	14799.652	-0.004
41.5	14799.996	-0.004
42.5	14800.345	-0.002
43.5	14800.694	-0.001
44.5	14801.047	0.000
45.5	14801.399	0.000
46.5	14801.753	-0.001
47.5	14802.111	-0.001
48.5	14802.468	-0.004
49.5	14802.830	-0.003
50.5	14803.201	0.004
51.5	14803.563	0.000
52.5	14803.931	-0.001
53.5	14804.302	0.000
54.5	14804.675	0.000

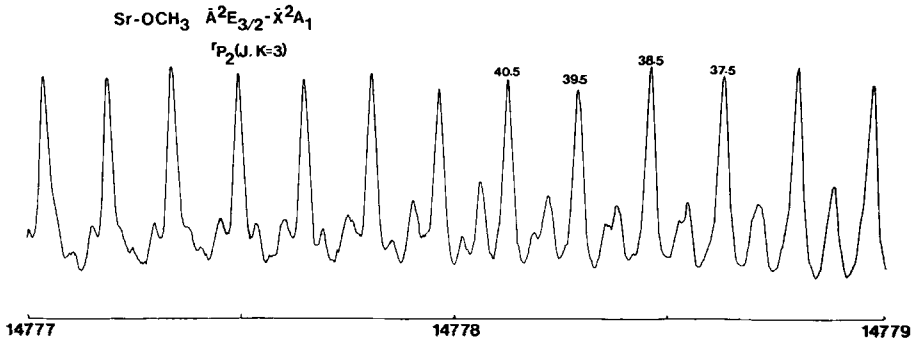

FIG. 3. High-resolution laser excitation spectrum of the $^rP_2$ (J, $K'' = 3$) branch of the O_0^0 band. The monochromator, set on the connecting Q_2 and P_{21} bandheads, acts as a narrowband-pass filter to select the lines from a single branch of a single subband.

As a result of the changes in bond order, the O–C vibrational frequency increases while the C–H frequencies decrease. These changes are manifestations of an effect called "anionic hyperconjugation" (*33, 34*).

TABLE III

The Molecular Constants for the 0–0 Band of the $\tilde{A}^2E$–$\tilde{X}^2A_1$ Transition of $SrOCH_3$ (cm^{-1})

A"	5.18511[a]
B"	8.39706(45) x 10^{-2} [b]
D_K"	4.151(29) x 10^{-3}
D_N"	1.07(10) x 10^{-6}
D_{NK}"	1.431(59) x 10^{-6}
ϵ_{aa}"	-1.78(38) x 10^{-3}
$\epsilon_{bb}+\epsilon_{cc}$"	1.586(28) x 10^{-3}
T_0'	14658.8721(9)
a_{SO}'	267.53(30)[c]
ζ_{ed}'	1.0[d]
ζ_t'	1.0[d]
A'	5.15244(16)
B'	8.50396(45) x 10^{-2}
D_K'	4.155(28) x 10^{-3}
D_N'	1.08(10) x 10^{-6}
D_{NK}'	1.261(62) x 10^{-6}
η_e'	2.95(17) x 10^{-6}
η_K'	1.676(10) x 10^{-2}

[a] Fixed to the value in Reference 23.

[b] One standard deviation uncertainty in parentheses.

[c] Estimated error, see the text for a discussion of the determination of the spin-orbit constant.

[d] Fixed to the value of 1.0, see the text.

There are four structural parameters for $SrOCH_3$, so some assumptions are required in order to extract a geometry from a single B_0 value. The photoelectron spectrum of CH_3O^- recorded by Engelking *et al.* (*35*) suggests that the C–O bondlength is similar for CH_3O^- and CH_3O. On this basis we choose r_{CO} = 1.376 Å from the microwave work of Endo *et al.* (*23*) on CH_3O. If we choose a CH bondlength of 1.0937 Å (assumed in Ref. (*23*)) and an H–C–H bond angle of 110.66° (derived in Ref. (*23*)) to match the OCH_3 values, then r_0 = 2.123 Å for Sr–O in the $\tilde{X}^2A_1$ state. In the excited $\tilde{A}^2E$ state r_0 = 2.104 Å for Sr–O and the H–C–H angle is 107.99°. This angle is derived from the A' value with ζ_t = 1 and the CH bondlength equal to 1.0937 Å. The Sr–O bondlength is thus 0.02 Å shorter in the excited state and H–C–H 2.7° smaller than in the ground state.

Consideration of the effects of anionic hyperconjugation will change these conclusions slightly but we are unable to find a suitable state-of-the-art ab initio calculation (large basis set and large scale configuration interaction). The C–O bondlength ranges from 1.33 to 1.40 Å in CH_3O^- crystal structures (*36, 37*). If the CH bondlength in $SrOCH_3$ is increased to 1.12 Å and the H–C–H angle decreased to 103°, then the Sr–O bondlength is 2.103 Å in the $\tilde{X}^2A_1$ state. These Sr–O bondlengths compare favorably with the Sr–O bondlength of 2.111 Å derived for the SrOH molecule. (*9*)

CONCLUSION

The rotational analysis of the 0–0 band of the $\tilde{A}^2E$–$\tilde{X}^2A_1$ transition of $SrOCH_3$ was carried out by laser excitation spectroscopy with narrowband fluorescence detection. This work is the first high-resolution analysis of a metal alkoxide molecule. The $\tilde{A}^2E$ state shows no sign of a Jahn–Teller effect. The Sr–O bondlength was found to be 2.12 Å, similar to the value in the SrOH molecule.

ACKNOWLEDGMENTS

This research was supported by the National Science Foundation (Grant CHE-8608630). Acknowledgment is made to the donors of the Petroleum Research Fund, administered by the American Chemical Society, for partial support of this research.

RECEIVED: July 17, 1987

REFERENCES

1. C. R. BRAZIER, P. F. BERNATH, S. KINSEY-NIELSON, AND L. C. ELLINGBOE, *J. Chem. Phys.* **82,** 1043–1045 (1985).
2. C. R. BRAZIER, L. C. ELLINGBOE, S. KINSEY-NIELSEN, AND P. F. BERNATH, *J. Amer. Chem. Soc.* **108,** 2126–2132 (1986).
3. L. C. ELLINGBOE, A. M. R. P. BOPEGEDERA, C. R. BRAZIER, AND P. F. BERNATH, *Chem. Phys. Lett.* **126,** 285–289 (1986).
4. L. C. ELLINGBOE AND P. F. BERNATH, *J. Amer. Chem. Soc.* **108,** 5017–5018 (1986).
5. C. R. BRAZIER AND P. F. BERNATH, *J. Chem. Phys.* **86,** 5918–5922 (1987).
6. A. M. R. P. BOPEGEDERA, C. R. BRAZIER, AND P. F. BERNATH, *J. Phys. Chem.* **91,** 2779–2781 (1987).
7. A. M. R. P. BOPEGEDERA, C. R. BRAZIER, AND P. F. BERNATH, *Chem. Phys. Lett.* **136,** 97–100 (1987).
8. R. F. WORMSBECHER AND R. D. SUENRAM, *J. Mol. Spectrosc.* **95,** 391–404 (1982).
9. J. NAKAGAWA, R. F. WORMSBECHER, AND D. O. HARRIS, *J. Mol. Spectrosc.* **97,** 37–64 (1983).
10. C. R. BRAZIER AND P. F. BERNATH, *J. Mol. Spectrosc.* **114,** 163–173 (1985).

11. Y. NI AND D. O. HARRIS, papers TG4 and TG5, 41st Ohio State University Symposium on Molecular Spectroscopy, 1986.
12. R. C. HILBORN, ZHU QINGSHI, AND D. O. HARRIS, *J. Mol. Spectrosc.* **97,** 73–91 (1983).
13. P. F. BERNATH AND S. KINSEY-NIELSEN, *Chem. Phys. Lett.* **105,** 663–666 (1984).
14. P. F. BERNATH AND C. R. BRAZIER, *Astrophys. J.* **288,** 373–376 (1985).
15. S. KINSEY-NIELSEN, C. R. BRAZIER, AND P. F. BERNATH, *J. Chem. Phys.* **84,** 698–708 (1986).
16. H. C. LONGUET-HIGGINS, U. OPIK, M. H. L. PRYCE, AND R. A. SACK, *Proc. R. Soc. A* **254,** 1–16 (1958).
17. J. T. HOUGEN, *J. Chem. Phys.* **37,** 1433–1441 (1962).
18. J. M. BROWN, *Mol. Phys.* **20,** 817–834 (1971).
19. J. T. HOUGEN, *J. Mol. Spectrosc.* **81,** 73–92 (1980).
20. J. K. G. WATSON, *J. Mol. Spectrosc.* **103,** 125–146 (1984).
21. H. E. RADFORD AND D. K. RUSSELL, *J. Chem. Phys.* **66,** 2222–2224 (1977).
22. D. K. RUSSELL AND H. E. RADFORD, *J. Chem. Phys.* **72,** 2750–2759 (1980).
23. Y. ENDO, S. SAITO, AND E. HIROTA, *J. Chem. Phys.* **81,** 122–135 (1984).
24. S. D. BROSSARD, P. G. CARRICK, E. L. CHAPPELL, S. C. HULEGAARD, AND P. C. ENGELKING, *J. Chem. Phys.* **84,** 2459–2465 (1986).
25. G. W. KING AND C. H. WARREN, *J. Mol. Spectrosc.* **32,** 138–150 (1969).
26. J. B. WEST, R. S. BRADFORD, JR., J. D. EVERSOLE, AND C. R. JONES, *Rev. Sci. Instrum.* **46,** 164–168 (1975).
27. M. DULICK, P. F. BERNATH, AND R. W. FIELD, *Canad. J. Phys.* **58,** 703–712 (1980).
28. G. HERZBERG, "Spectra of Diatomic Molecules," 2nd ed., pp. 257–264, Van Nostrand–Reinhold, New York, 1950.
29. G. HERZBERG, "Electronic Spectra and Molecular Structure of Polyatomic Molecules," Van Nostrand–Reinhold, New York, 1966.
30. E. KAUFMAN, P. V. R. SCHLEYER, K. N. HOUK, AND Y. D. WU, *J. Amer. Chem. Soc.* **107,** 5560–5562 (1985).
31. M. L. STEIGERWALD, W. A. GODDARD III, AND D. A. EVANS, *J. Amer. Chem. Soc.* **101,** 1994–1997 (1984).
32. For example, D. A. WEIL AND D. A. DIXON, *J. Amer. Chem. Soc.* **107,** 6859–6865 (1985), or A. PROSS AND L. RADOM, *J. Amer. Chem. Soc.* **100,** 6572–6575 (1978).
33. F. A. SEUBOLD, JR., *J. Org. Chem.* **21,** 156–160 (1955).
34. E. MAGNUSSON, *J. Amer. Chem. Soc.* **108,** 11–16 (1986).
35. P. C. ENGELKING, G. B. ELLISON, AND W. C. LINEBERGER, *J. Chem. Phys.* **69,** 1826–1832 (1978).
36. A. BINO, *J. Amer. Chem. Soc.* **109,** 275–276 (1987).
37. H. STAEGLICH AND E. WEISS, *Chem. Ber.* **111,** 901–905 (1978).